Rapid prototyping and immunogenicity of SARS-CoV-2 DNA vaccine candidates formulated with the Fusogenix proteo-lipid vehicle delivery system.

Arun Raturi[1,2], Ping Wee[1,2], Prakash Bhanduri[1,2], Manoj Parmar[1,2], Douglas Brown[3], Maryam Hejadi[3], Liliya Grin[1,2], Hector Vega[1,2], Jennifer Gyoba[1,2], Jailal Ablack[1,2], Katia Carmine-Simmon[3], Perrin H Beatty[1,2], Alyson Kelvin[4], Roy Duncan[4], John D Lewis[1,2,3] **

Affiliations
[1] Entos Pharmaceuticals, 4550 - 10230 Jasper Avenue, Edmonton, Alberta, Canada, T5J 4P6
[2] Aegis Biodefense, 3033 Science Park Road, San Diego, California, 92121
[3] Department of Oncology, University of Alberta, Edmonton, Alberta, Canada, T6G 2E1
[4] Department of Immunology, Dalhousie University, Halifax, Nova Scotia, Canada, T6G 2E1

**Correspondence to: John D. Lewis. University of Alberta, Katz Group Centre, 5-142, Edmonton, Canada. Phone: 780.492.6113, Fax: 780-492-8160, Email: (10)(2e) @ualberta.ca

Subject Areas: Vaccine development, Infectious diseases

Keywords: SARS-CoV-2, COVID-19, DNA vaccine, Fusogenix, Proteo-lipid vehicle, neutralizing antibodies, preclinical

One sentence summary: Rapid prototyping and selection of pan-coronavirus DNA vaccine candidates optimized to maximize neutralizing antibody and balanced T helper cell response and minimize antibody-dependent enhancement.

Abstract

Here we describe the development and evaluation of a panel of DNA vaccine candidates (Covigenix) formulated with the Fusogenix proteo-lipid vehicle (PLV) platform, a nanoparticle formulation that utilizes fusion-associated small transmembrane (FAST) proteins to drive direct fusion of lipid-encapsulated plasmid DNA with the plasma membrane of target cells. A rapid prototyping approach was employed to evaluate sequences encoding the full-length SARS-CoV-2 spike (S) protein, native and secreted versions of the receptor binding domain (RBD), or the full-length nucleocapsid (N) protein. The addition of genetic-encoded adjuvants RIG-I and CpG was evaluated, with the overall goal of stimulating potent neutralizing antibody and/or balanced cell-mediated responses while minimizing the risk of antibody-dependent enhancement.

In preclinical immunogenicity studies at doses ranging from 5 μg to 100 μg, it was found that candidates encoding SARS-CoV-2 full length spike stimulated the most robust neutralizing antibody titers, and that incorporation of genetic RIG-I and CpG adjuvants significantly improved responses. The secreted RBD also stimulated a strong neutralizing antibody response compared to the non-secreted version, while the N protein-encoded candidates did not stimulate a strong antibody-mediated response. Serum from mice immunized with a 25 μg dose of the Covigenix full length spike candidate with genetic adjuvants produced a neutralizing titration curve similar to that derived from a panel of COVID-19 convalescent patients.

Several of the vaccine candidates elicited a robust and sustained expansion of the B cell compartment in the spleen, as assessed by immunophenotyping of cell-mediated immune cell populations following vaccination. The Covigenix N-protein vaccines produced the strongest T-cell responses, with significant activated CD8+ cells in the peripheral blood and the spleen 3 days and 14 days post-immunization, while the full length spike vaccines showed a significant increase in antigen-specific IFN-gamma producing T cells as well as activated CD8+ lymph node cells.

Based on this preclinical data, Covigenix candidates encoding full length S and N proteins will be advanced to human clinical trials. While the S vaccine simulates both an antibody and T-cell response, the N vaccine seems to be a potent T-cell vaccine that has the potential for pan—coronavirus activity. These candidates will now be evaluated in SARS-CoV-2 animal challenge studies and advanced to phase 1/2 human clinical trials starting this summer, leading towards phase 3 trials shortly afterwards.

Introduction

SARS-CoV-2, the causative agent of COVID-19, has infected over 12.4M people, caused over 557K deaths, over-burdened healthcare systems, and led to unemployment and food shortages in various regions of the world. The global impact of the current coronavirus (CoV) pandemic is unprecedented, and without vaccine protection, is predicted to continue. Currently, the only countermeasures to reduce SARS-CoV-2 infection rates are mobility restriction and social distancing. However, these measures are not sustainable and do not provide protection from COVID-19 like a vaccine can. Besides SARS-CoV-2, our enemy is time: every day without a protective COVID-19 vaccine means more deaths, worldwide (*1*).

SARS-CoV-2 is the third most recent betacoronavirus zoonosis, after the initial 2003 SARS (9.6% fatality rate) and the 2012 MERS (35% fatality rate) coronavirus outbreaks, to cause human-to-human transmission and acute respiratory distress syndrome (ARDS). Betacoronaviruses are enveloped viruses with four major structural proteins, spike surface glycoprotein (S), envelop (E), membrane (M), and nucleocapsid (N), encasing the 29.9 Kbp positive sense RNA genome (Figure 1) (*2*). Homotrimers of the S protein form the spikes on the CoV surface that bind to host cell receptors, such as the angiotensin converting enzyme 2 (ACE2) receptors with SARS-CoV-2. Therefore, CoV S proteins initiate virus – host cell fusion and entry, which ultimately determines host range and zoonosis. spike proteins comprise two subunits (S1 and S2). S1 contains the highly variable host-specific receptor binding domain while S2 is highly conserved across CoV strains and carries the fusion peptide, transmembrane domain and cytoplasmic domain. The spike protein also has a polybasic amino acid sequence that acts a cleavage site for the human protease furin. Spike protein cleavage by the furin protease is essential for effective SARS-CoV-2 binding, fusion and host cell entry (*3*). The N abundantly expressed, and highly conserved, CoV N protein binds, packages and maintains the viral RNA genome in long helical ribonucleoprotein structures that are also in proper conformation for viral genomic replication and transcription to occur (*4*). Recent studies also show N protein involvement in regulation of host cell processes like actin reorganization, cell cycle progression, and apoptosis (*5*).

SARS and SARS-CoV-2 immune studies show that the N protein can induce protective immune responses against these viruses during infection and as a vaccine antigen with predominant B cell epitopes (*6-9*). SARS immune studies with spike protein stimulated host

system neutralizing antibody production, making it a promising antigen candidate for neutralizing antibody vaccines. However, this protein also elicited non-neutralizing antibodies that promoted an antibody-dependent enhancement (ADE) of disease upon re-infection with SARS (*10*). ADE was also observed after vaccination for respiratory syncytial virus (RSV) (*11-14*). In these cases there was a skewed T helper cell response after vaccination and viral challenge which lead to increased eosinophil pathology in the respiratory tract and hepatitis at challenge (*8*). Recent studies show that antigens eliciting a balanced T helper cell type 1 (Th1) and T helper cell type 2 (Th2) directed immune response have a reduced likelihood of ADE.

We initiated a rapid prototyping protocol to generate nanoplasmid (NTC) or p10 expression vector DNA encoded SARS-CoV-2 and pan-coronavirus full length (FL) S protein, S protein wildtype receptor binding domain (RBD1, 2, 3) and secreted RBD (sRBD), and FL N protein epitopes as the payload optimized to maximize neutralizing antibody and balanced T helper cell response to minimize ADE. Retinoic acid-inducible gene I (RIG-I) and unmethylated CpG motifs were also included as payloads for codelivery to host cells to act as nucleic acid adjuvants to stimulate innate immune responses and drive adaptive Th1 responses (*15*). RIG-I is a cytoplasmic double-stranded RNA pattern receptor. Activation of RIG-I leads to type I interferon (IFN) and inflammatory cytokine production (*16-18*). Unmethylated CpG motifs can also stimulate innate immunity and improve adaptive immunity against the antigen gene product (*19-22*).

The plasmid DNA payload was encapsulated within Fusogenix, a proprietary proteo-lipid vehicle (PLV) formulated with well-tolerated neutral lipids and proprietary p14 protein that ensures highly efficient fusion and intracellular delivery of nucleic acid payloads directly into cells to drive potent immune responses (Figure 1A,E) (*23-29*). Fusogenix has undergone extensive pre-clinical studies in rodents and non-human primates and been shown to be safe and highly effective for *in vivo* nucleic acid delivery. Fusogenix is non-immunogenic, allowing for repeat dosing with no reduction in efficacy, delivers payloads to a wide variety of extra-hepatic tissues and cell types (including antigen presenting cells), and is well tolerated at doses 10x the expected human efficacious dose (*30*). The technology is also inexpensive and scalable, making it ideal for vaccine production.

In total, we evaluated 24 potential COVID-19 DNA vaccine candidates for levels of neutralizing antibody and T cell immunity measured in a 1 or 2-dose vaccine candidate regimen

over 28 days in preclinical mouse studies. Two DNA vaccine candidates showed potent neutralizing antibody and balanced T helper cell responses and inhibition of viral infection. These preclinical results demonstrate that our lead Fusogenix DNA vaccines, encoding a combination of SARS-CoV-2 FL-S, FL-N, and conserved coronavirus antigens that enhance the vaccine's potency and provides broad based immunogenicity to SARS-CoV-2, are promising DNA vaccine candidates against COVID-19.

Results

Covigenix DNA vaccine candidates were assessed for their safety, immunogenicity, and efficacy against SARS-CoV-2 in mouse models. Based on the results reported here two vaccine candidates were selected to advance to CTA-enabling, preclinical safety/tolerability studies and GLP toxicity studies in non-human primates (NHP) at multiple dose levels and schedules.

Design and construction of Covigenix plasmid DNA vaccines

We selected theSARS-CoV-2 spike glycoprotein, the spike RBD, and the nucleocapsid for the Coivgenix vaccine candidate antigens (*31*). Human codon optimized full length DNA sequences were synthesized based on the published amino acid sequences (QHD43416) of the SARS-Cov2 spike protein and N protein and cloned into either our standard p10 expression vector or one of two nanoplasmid vectors from Nature Technologies either without adjuvant sequences (NTC) or with un-methylated CpG sequences and a RIG-I agonist element (NTC-RIG-I). The sequence encoding the wildtype SARS-CoV2 spike Receptor Binding Domain (RBD) was also cloned into the p10 vector as well with the following modifications: 1) Addition of IgG heavy chain signal sequence resulted in a secreted RBD (sRBD-1) or 2) point mutations intended to stabilize the RBD conformation (RBD-2 and RBD-3).

Humoral Immunity Induced by Covigenix Vaccine Candidates

The aforementioned plasmid DNA vectors were encapsulated with the Fusogenix delivery platform. A group of mice were immunized IM with each candidate using a prime (day 0)-boost (day 14) regimen. Seven days following the boost dose (day 21) serum anti-spike IgG concentration was measured by ECLIA assay with recombinant spike protein. spike-NTC with RIG-I elicited nearly 6000 ng/ml of anti-spike antibody, versus approximately 3000 ng/ml of

anti-spike antibody from spike-NTC lacking the nucleic acid adjuvant and 2000ngml from sRBD-CpG at similar doses (Figure 2A, B). The p10 vector expressing full length spike also enabled anti-spike antibody production but at a lower level. Even at 4 times the dose (100ug) the p10 vector was unable to stimulate antibody production equivalent to the NTC vectors. The addition of unmethylated CpG oligo nucleotides (co-formulated) with the plasmid DNA vector improved antibody production but again not to level of the NTC vectors (Figure 2A). Vaccine formulations encoding the wild type RBD domain of SARS-Cov2 spike protein elicit a lower concentration of anti-spike antibodies compared to vectors encoding the full length spike protein. A secreted RBD domain stimulated the best response among RBD constructs at dose of only 25ug (Figure 2B). The sRBD construct performed as good as or better than the FL-spike protein in the same vector backbone (Figure 2B). The NTC-spike candidates elicit the most robust spike antibody responses, achieving serum antibody concentrations equivalent to the primed and boosted p10 vectors (both FL-spike and RBD constructs) after a single dose for the RIG-I version (Figure 2C). Furthermore, antibody production prior to the booster dose with spike NTC-RIG-I was nearly equivalent to the boosted level using spike-NTC and the RIG-I nucleic acid adjuvant resulted in an even greater increase following the boost dose (Figure 2C). Consistent with the robust serum antibody concentrations from spike protein expressed from NTC vectors, the spike-NTC Covigenix candidates also elicit robust and sustained expansion of the B cell compartment in the spleen following the booster dose (Figure 2C). The B cell expansion induced by Covigenix spike protein candidates was indistinguishable from that of a known model immunogen, firefly luciferase (NTC-Luc) (Figure 2D).

Neutralizing Antibody Production

Pseudotyped high risk group (RG-3 and 4) viruses are a safe viral entry model to perform antibody screens and neutralizing titer assays because they do not produce infectious progeny (*32*). Vesicular Stomatitis Virus (VSV), entry is dependent on its surface glycoprotein (G protein). Replacement of the VSV G gene with a green fluorescence protein (GFP) reporter in the VSV genome renders VSV entry dependent on glycoproteins from other viruses, such as SARS-CoV-2 spike, supplied in trans during virus growth and provides a convenient reporter for infected cells. A recent preprint measured the neutralizing titer from COVID-19 convalescent patient sera with an *in vitro* SARS-CoV-2 pseudotyped assay and reported good correlation with

live SARS-CoV-2 assays (*33*). Neutralizing properties of the immunized mouse serum was determined using a GFP reporter VSV, pseudotyped with wild-type SARS-CoV-2 spike protein. SARS-CoV-2 FL-spike pseudotyped recombinant VSVdG-GFP was incubated with serial dilutions of heat inactivated serum from immunized mice and used to infect permissive 293TT-ACE2 overexpressing cells (*17*). The neutralizing antibody titer is measured by counting the GFP positive cell numbers after 12 hours of infection. The serum from spike-NTC RIG-I, spike plus CpG, and sRBD plus CpG immunized mice was tested for neutralizing titer in parallel with 19 convalescent human serum samples and a Sars-Cov-2 negative human serum control sample. Non-immunized control and the negative human serum showed no detectable inhibition compared to uninfected cells. Serum from mice immunized with spike-NTC-RIG-I showed a neutralizing titration curve similar to convalescent patients both with an IC50 titer greater than 1 in 100. Serum from p10 spike-CpG and sRBD-1-CpG immunized animals showed lower titers with IC50 values around 1in10. Thus, spike-NTC+RIG-I Covigenix vaccine elicits a similar neutralizing antibody profile to that of convalescent patients (Figure 3).

Induction of cytotoxic T lymphocyte (CTL) response

Next, we examined cell mediated immunity with our lead candidates. Mice were injected intramuscularly with a 25μg dose of Fusogenix with a payload encoding FL-spike-NTC with or without RIG-I or saline control on day 1 (prime) and day 14 (boost). At 21 days post immunization (7 days following the booster), mouse splenocytes were stimulated *ex vivo* with overlapping peptide pools (15mers overlapping by 11) spanning the entire SARS-CoV2 spike protein open reading frame in (ORF) in two pools to determine the frequency of antigen specific spot forming cells (SFC) per million ± SEM from each immunized animal. The FL-spike-NTC+RIG-I DNA vaccine candidate showed a significant increase in IFNγ-expressing spot forming cells per million splenocytes compared to the unimmunized control for both peptide pools (Figure 4A). The spike-NTC vaccinated animals produced a detectable increase in the frequency of antigen-specific IFN gamma producing T cells that trended toward significance. Immunophenotyping of CTL populations following vaccination with spike-NTC+RIG-I, spike-NTC and the model antigen Luc-NTC showed an increase in activated (CD69+) CD8+ CTLs present in the lymph nodes 3 days (day17) and 14 days (day 28) post immunization (Figure 4B). There is a concurrent expansion of the CD8 T cell compartment in the spleen 3 days (day 17) and

14 days (day 28) post boost (Figure 4C). Covigenix spike-NTC vaccine candidates elicit a balanced humoral and cell mediated response.

Nucleocapsid-protein as a pan-Coronavirus Vaccine candidate.

The CoV N is an attractive pan coronavirus vaccine candidate because it is the most highly conserved (91%) protein among beta-coronaviruses (*4*). Furthermore, in other RNA viruses, including VSV, the nucleocapsid protein is effectively present via MHC class I and targeted by CTLs. Based on the ability for Covigenix vaccines to elicit cell mediated immunity we also developed Covigenix vaccine candidates expressing the SARS-CoV-2 N protein expressed from NTC vectors. Consistent to spike protein candidates, Covigenix N-protein vaccines activate CD8 cells in the periphery (CD69+) and also in the spleen 3 days and 14 days post immunization similar to that of model antigen (fig5A,B). Therefore, the Covigenix vaccine platform could elicit a pan coronavirus vaccine targeting cell mediated immunity against N protein.

Discussion

In terms of infection, mortality, and economic disruption, the global impact of the COVID-19 pandemic is unprecedented. We need effective and safe vaccines that induce neutralizing antibodies against SARS-CoV-2 and protect against pan- coronavirus threats. The World Health Organization (WHO) global vaccine candidate landscape and the Milken Institute vaccine tracker list 160 and 192 COVID-19 vaccines in development around the world, respectively(Table 1) (*34, 35*). The majority of these are protein subunit vaccines, which is unsurprising considering that this type of antigen platform has been used before to make Hepatitis B and shingles vaccines and, along with virus-like particle (VLP), are considered safer than using live-attenuated virus or inactivated virus as antigenic platforms(*36-38*). However, these four antigen platform types all take a lengthy amount of time to develop and validate, which is detrimental to developing a vaccine against an emergent, pandemic virus. The next major antigen platform types being used in development of COVID-19 vaccines involve using either non-replicating or replicating viral vectors for SARS-CoV-2 antigen delivery. Although these platforms are faster to develop than protein subunit vaccines, they have the disadvantage that the viral vector is immunogenic, therefore these vaccines cannot be effectively re-administered after one dose. Interestingly, 40 of the developmental COVID-19 vaccines

recognized by the Milken Institute are RNA or DNA vaccines; both types introduce a plasmid encoding antigens able to promote an immune response, directly into the recipient's cells so that the target antigen is produced by those cells. These platforms are next-generation, disruptive technologies that are poised to revolutionize medicine, but have not been approved for human vaccine use yet (*39-49*).

Both RNA and DNA vaccine platforms offer many advantages over traditional platforms; optimization of gene-encoded epitopes to eliminate ADE, rapid development time, ease of large-scale manufacturing, absence of any infectious agent, and the stimulation of both humoral and cell-mediated responses. However, DNA vaccines offer further advantages over RNA vaccines such as expression of multiple epitopes, more stable and less costly to develop (Table 1). Proof-of-concept has been established in nonhuman primates with pan-influenza virus DNA vaccines(*50, 51*). Clinical trials show that DNA vaccines are safe and that they can evoke cellular and humoral immune responses(*52*). A major barrier to DNA vaccine development is the method of intracellular delivery. Some DNA vaccines use an adenovirus vector for delivery, which has been proven to be immunogenic, limiting the vaccine to single dose use and other viral vector vaccines cannot be used by the recipient(*21, 53, 54*). Other DNA vaccines require recipient electroporation with a handheld electric device for effective delivery.(*55*). However, our Fusogenix delivery platform removes that barrier by allowing for efficient, non-immunogenic, and non-toxic delivery of DNA payload directly into the host cell cytoplasm(*17, 18, 24, 29, 41, 56-70*).

We initiated a rapid prototyping and iterative optimization of a pan-coronavirus DNA vaccine payload to maximize the neutralizing antibody and balanced Th-response and minimize ADE response. A panel of 24 recombinant plasmid DNA vaccines were engineered to encode combinations of FL-S, secreted S, sRBD, optimized S epitopes from CoV and SARS-COV-2, retinoic acid-inducible gene I (RIG-I) and unmethylated CpG motifs. FL-spike with RIG-I at 25 ug dose elicited nearly 6000 ng/ml of anti-spike antibody, as did a two-dose (prime plus boost) vaccination regime. The Covigenix DNA vaccine with nanoplasmid encoding FL-spike with RIG-I produced equivalent neutralizing antibody titer to convalescent COVID-19 patients. The same Covigenix candidate showed significant increase in IFNγ-expressing spot forming cells per million splenocytes indicating that it is a potent generator of T cells that have the potential to destroy SARS-CoV-2 infected host cells.

Materials and Methods

Recombinant Plasmid Construction

Antibiotic free nanoplasmid NTC9395R-eRNA41H-CpG RNA (NTC, Lincoln, NE) was used as the vector for cloning the 3822bp human codon optimized SARS-CoV-2 FL-spike (S) gene (synthesized by Integrated DNA technology; Iowa, USA) using *Sal*I and *Bgl*II restriction sites. Transgene expression was driven by the chimeric CMV promoter, with a rabbit beta-globin intron and splice enhancer for efficient RNA export. Rabbit beta-globin polyA signal was used for mRNA transcriptional termination and polyadenylation. RNA Pol III-expressed eRNA41H serves as a pathogen-associated molecular pattern (PAMP) recognized by cytoplasmic retinoic acid-inducible gene 1 (RIG-I) receptor (*16*). RNA pol II driven CpG RNA is efficient activator of NF-κB and p38 MAPK (*22*).

Covigenix DNA vaccine formulation

To manufacture Covigenix DNA vaccines, plasmid DNA was encapsulated by Fusogenix. Plasmid DNA was diluted in 10 mM sodium acetate buffer (pH 4.0) containing 5 nM Fusogenix p14 protein. Separately, the Fusogenix lipid components was dissolved in ethanol. Microfluidic mixing of the DNA-protein fraction with the lipid fraction was performed by NanoAssemblr Benchtop (Precision Nanosystems Inc, Vancouver, BC) at a ratio of 3:1 at 12 mL/min. Formulations were dialyzed in 8000 MWCO dialysis membranes (BioDesign, Carmel, New York) against phosphate-buffered saline (pH 7.4) for 3 hours with 3X buffer changes, then concentrated by Amicon ultracentifuge filters (EMD Millipore, Burlington, Massachusetts) before being passed through a 0.22 µm filter (EMD Millipore). The resulting Covigenix DNA vaccine candidates were stored at 4°C until use. Covigenix DNA candidates were also tested for particle size, zeta potential, and plasmid DNA encapsulation. PLV mean size was between 80-120 nm, zeta potential was between -0.1 and -0.2 mV, and encapsulation efficiency was >85%.

Animal Experiments: Ethics and Study Design

All animal studies were carried out according to the guidelines of the Canadian Council on Animal Care (CCAC) and approved by the University of Alberta Animal Care and Use Committee. *In vivo* studies were done using 8-20 weeks old, 25 to 35 g body weight, male and female C57BL/6 (Charles River Laboratories, Saint-Constant, QC, Canada). Animals were group housed in IVCs

under SPF conditions, with constant temperature and humidity with lighting on a fixed light/dark cycle (12-hours/12-hours).

Mice were immunized intramuscularly (IM) in the musculus tibialis with 50µl of test agent, unless otherwise stated. Baseline blood was collected via tail vein prior to immunization. Blood was collected again 14 days after initial immunization immediately prior to booster administration. Twenty-one days after immunization mice were euthanized and terminal blood was collected. For the ELISpot experiments animals are sacrificed 21 days after initial immunization. Spleens are removed and dissociated into single cell suspensions using Spleen Dissociation Kit (Miltenyi Biotec; Auburn, CA) by following the manufacturer protocol.

Anti-spike Antibody Titer: Indirect ELISA with Sera from Immunized Mice

Recombinant SARS-COV-2 spike S1 Protein (ABclonal, Wuhan, China) was coated on the standard binding plate (Meso Scale Discovery; MSD, Rockville, MD) at 1 µg/mL for 1 h at room temperature (RT) on shaker. The plate was washed three times with 0.05% Tween-20 in PBS (PBS-T, In-house prepared) followed by addition of Blocker A (blocking buffer, MSD). After 30 min of incubation, the plate was washed again with PBS-T. Serially diluted SARS-CoV-2/SARS-CoV spike Antibody Standards (Cat. No. 3223, ProSci Inc, San Diego, CA) were prepared in Blocker A. Covigenix DNA candidate-immunized mouse serum samples were diluted 1:100 in Blocker A. The antibody standards and diluted mouse serum samples were loaded to plates and incubated for 1 h at RT on shaker. The plate was washed again with PBS-T followed by addition of 1 µg/mL Sulfo-tag Anti-Rabbit Secondary Antibody in standards (Meso Scale Discovery; MSD, Rockville, MD), and 1 µg/mL Sulfo-tag Anti-Mouse Secondary Antibody in Mouse serum samples (Meso Scale Discovery; MSD, Rockville, MD). Read buffer (Meso Scale Discovery; MSD, Rockville, MD) was added to the plate after washing with PBS-T, and the plate was read in MESO QuickPlex SQ 120 (Meso Scale Discovery; MSD, Rockville, MD).

Preparation of VSV-S pseudotyped virus

Neutralizing antibody responses were assessed using vesicular stomatitis virus (VSV) lacking the VSV G receptor binding protein and pseudotyped with the SARS-CoV-2 S protein. To generate the pseudotyped virus 293T cells were transfected with plasmid pMD2.G (Addgene) expressing

the VSV-G protein and 24 h later transduced with a VSV-G pseudotyped VSVdeltaG-GFP virus. The supernatant from cells containing VSV virions pseudotyped with VSV-G was harvested at 24 h post-transduction, clarified by centrifugation at 500 x g for 5 min and aliquots stored at -80°C. This virus was used to infect 293T cells transfected the previous day with pcDNA3 expressing a codon-optimized version of the SARS-CoV-2 S protein (accession #YP_009724390.1) with a truncated cytoplasmic tail missing the C-terminal 19 amino acids. Virus inoculum was removed after 1 h at 37°C, cells were washed twice with PBS, incubated in growth medium for 24 h and the supernatant removed and clarified by centrifugation at 500 x g for 5 min before freezing the stock aliquots at -80°C. These stocks of VSV-S pseudotyped virions were subsequently used for antibody neutralization assays.

Pseudotype neutralization assay

Vero cells were seeded in 96-well plates at $5x10^3$ cells/well and incubated overnight at 37°C. Mouse serum from vaccinated animals and human convalescent serum from SARS-CoV-2 infected patients, previously heat inactivated at 56°C for 30 min and stored at -80°C, was serially diluted in serum free media (1:5, 1:10.1:30, 1:80, 1:150) and 50ul aliquots mixed with 50 ul of the VSV-S pseudotyped virus inoculum, sufficient to produce ~200 infected cells per field of view at 200x magnification. Virus-antibody mixtures were incubated at 37°C for 1 h, added to the Vero cells for 1 h at 37°C, and then the virus inoculum was removed, cells were washed with PBS and incubated in growth medium for 10 h at 37°C. Cell monolayers were imaged at 200X using an EVOS model cell imaging system (ThermoFisher Scientific, Waltham, MA) and the number of fluorescent cells in 3 random fields from each well quantified using ImageJ software.

Interferon-Gamma ELISpot

Spleens from immunized mice were collected aseptically and homogenized into single cell suspensions in complete media (RPMI1640 media supplemented with 10% FBS, penicillin/streptomycin and 1x BME). Cells were collected by centrifugation at 1500 x g for 5 minutes and pellets were re-suspended in 1 mL of ACK lysis buffer (Life Technologies, Carlsbad, CA). Following an 8 min incubation at RT, complete media was added to stop the reaction. Cells were again collected by centrifugation at 1500 × g for 5 min and resuspended in fresh complete media and passed through a 70 µm nylon filter. Single cell suspensions were

counted and resuspended at 2 x10^6 cells/ml for use in the ELISpot assay. Mouse IFN-γ ELISpot assays were performed using the Mouse IFN-γ ELISpot Kit (R&D systems, Minneapolis, MN) according to the manufacture's directions.

Briefly, 96-well ELISpot plates pre-coated with capture antibody were hydrated with complete media for 2 hours at room temperature, followed by incubation with streptavidin-AP concentrate for 2 hours at room temperature. Color is developed with BCIP/NBT substrate addition for one hour at room temperature. 2.0x10^5 mouse splenocytes were plated into each well and stimulated at 37°C for 18 h with PepMix™ SARS-Cov-2 spike peptide pools at a final concentration of 1.5nM (JPT, Berlin, Germany). PepMix™ pools consist of 15-mer peptides overlapping by 11 amino acids spanning the entire open reading from of SARS-COV2 spike protein divided into two peptide pool. Unstimulated cells served as control. Plates were allowed to dry for 2 days then spots were scanned and quantified by ImmunoSpot S6 MACRO Analyzer (CTL, Cleveland, Ohio). Assays were performed in duplicate (for each donor mouse). To calculate Spot-Forming Cells (SFC) per million ± SEM, mean spot counts from control unstimulated splenocytes were subtracted from the representative SARS-CoV-2 spike stimulated splenocyte sample.

Statistical analyses

The statistics were calculated using GraphPad Prism 5.0 program. Statistical differences between the control and experimental groups were analysed using one-way ANOVA and Tukey's multiple comparison test and were considered significant for $p< 0.05$.

Figures and Tables

Figure 1 Sequence features of SARS-CoV-2. A) Depiction of p14 Fusion-Associated Small Transmembrane (FAST) protein. B) The complete whole genomic features of SARS-CoV-2 isolate Wuhan-Hu-1 (Genebank: MN908947). UTR: untranslated region; orf/ORF: open reading frame; TRS: transcriptional regulatory sequences; S: spike glycoprotein encoding region; E: envelope protein encoding region; M: membrane protein encoding region; N: nucleocapsid protein encoding region. The figure is illustrated by SnapGene Viewer. C) 2D Domain architectures and 3D ribbon diagrams of SARS-CoV-2 spike and D) nucleocapsid proteins. NTD: N-terminal RNA binding domain; CTD: C-terminal dimerization domain.(*4*) E) Diagram

of Fusogenix PLVs fusing with the target cell and delivering the DNA payload directly into the cytoplasm. F) Flow diagram of the Covigenix DNA vaccine candidates with FL-spike, spike RBD, and FL-N genes encoded on nanoplasmid vectors.

Figure 2. Induction of antibody responses by Candidate Covigenix vaccines. Mice were immunized intramuscularly (IM) on Day 1 and 14 with either a 25 ug or 100 ug dose of candidate plasmid DNA vaccines with the Fusogenix platform. The concentration of elicited anti-spike protein antibodies was measured by immunoassay on the meso-scale discovery (MSD) Platform. A) Inset: schematic diagram of SARS-CoV2 spike protein. Graph of plasmid DNA candidates encoding full length spike protein expressed with and without the Nanoplasmid cassette (NTC) and with or without the RIG-I sequence. B) Inset: schematic diagram of SARS-CoV-2 spike protein Receptor Binding Domain (sRBD). Graph with plasmid DNA candidates encoding sRBD with and without CpG sequence. C) Antibody production by Covigenix candidates 14 days following a single dose (Prime) or 7 days following a second dose (Prime+Boost). D) Percent CD19 plus TCR-Beta- cells at Days 14, 17 and 28 in the Covigenix spike protein candidates versus a known model immunogen, firefly luciferase (NTC-Luc).

Figure 3. The neutralizing titer of serum from spike-NTC RIG-I, spike plus CpG, and sRBD plus CpG immunized animals (n=1 each) was determined using VSV-deltaG-GFP backbone pseudotyped with SARS-CoV-2 S protein neutralization assays in permissive 293TT-ACE2 cells. For comparison convalescent human serum samples were tested in parallel (n=19). A Sars-Cov-2 negative human serum sample was used as a control. The graph depicts the percent change from the Covigenix DNA vaccine candidates compared to untreated control as the percent infection reduction ±SEM.

Figure 4: Induction of cytotoxic T lymphocyte (CTL) responses from Covigenix DNA vaccine candidates were evaluated using ELISpot assays. A) Mice were immunized with either spike-NTC-RIG-I, spike-NTC or Control (n=3 per group) on day 1 (prime) and day 14 (boost). At 21 days post immunization (7 days following the booster), the mouse splenocytes were stimulated ex vivo with overlapping peptides spanning the entire SARS-CoV2 spike protein open reading frame (ORF). Interferon gamma producing cells were measured by enumerating the antigen

specific spot forming cells (SFC) per million ± SEM for each peptide pool. * denotes significant difference from control $P<0.05$ by One-Way ANOVA and Tukeys multiple comparison test. Inset: scale diagram of the Sars-Cov2 spike protein indicating the regions covered by each peptide pool. B) Immunophenotyping of CTL populations following vaccination with spike-NTC+RIG-I, spike-NTC and the model antigen Luc-NTC showed an increase in activated (CD69+) CD8+ CTLs present in the lymph nodes 3 days (day17) that dropped off by 14 days (day 28) post immunization. C) There was a concurrent expansion of the CD8 T cell compartment in the spleen 3 days (day 17) and 14 days (day 28) post boost.

Figure 5: Immunophenotyping of CTL populations following vaccination with A) N Protein-NTC+RIG-I N Protein-NTC, and the model antigen Luc-NTC showed an increase in activated (CD69+) CD8+ CTLs present in the lymph nodes 3 days (day17) but not 14 days (day 28) post immunization. C) There was a concurrent expansion of the CD8 T cell compartment in the spleen 3 days (day 17) and 14 days (day 28) post boost.

Table 1. COVID-19 vaccines in development. The number of vaccines at the stage of: Preclinical (PRE), Human Clinical Trial I, II, or III, Regulatory Review (RR), or Clinical Phase IV as of July 12, 2020. References listed for vaccine candidates in any clinical stage with a preprint or peer reviewed publication. Adapted from the WHO COVID-19 draft vaccine landscape and the Milken Institute (*35, 71*).

			Stages							Total
Platform	Advantages/Examples	Limitations/Challenges	PRE	I	II	III	RR	IV	Ref	
Protein subunit	Non-infectious Examples: Hepatitis B and shingles.	Take considerable time to develop and validate, not timely for pandemic response.	59	3						**62**
RNA	Can be developed more quickly and easily than other vaccines	RNA vaccines are expensive, unstable (must be stored at -80C), and toxic (positive charges). No RNA vaccines have been approved for human use.	21	3	1				(*72, 73*)	**25**
Non-Replicating Viral Vector	Cannot cause disease.	Immune response against the delivery platform; cannot repeat dose and other viral vector vaccines cannot be used by the recipient. No approved product of this kind has resulted to date.	20	**1**	1	1			(*74*)	**23**
Replicating Viral Vector	Examples: Ebola and Dengue.	Immune response against the delivery platform; cannot repeat dose and other viral vector	17							**17**

		vaccines cannot be used by the recipient.								
DNA	Can be developed more quickly and easily than other vaccine types. Fusogenix DNA vaccines are nonimmunogenic and non-toxic, allowing for multiple dosing of the same vaccine and repeated use for other vaccines.	DNA vaccines using a viral vector can cause an immune response – no repeat dosing and other viral vector vaccines cannot be used by the recipient. Some DNA vaccines need electroporation with a handheld device (massive electric charge) to allow DNA entry into the cell. No DNA vaccines have been approved for human use yet.	13	2					(*75*)	**15**
Virus-Like Particle (VLP)	Safer alternative to attenuated viruses. Example: HPV vaccine.	Take considerable time to develop and validate, not timely for pandemic response.	14							**14**
Inactivated virus	Can be given to people with weakened immune systems. Examples: polio and influenza	Take considerable time to develop and validate, not timely for pandemic response. Could cause disease if not fully inactivated.	**8**		**4**				(*76*, *77*)	**12**
Live attenuated virus	Elicit a strong immune response. Examples: measles, mumps, and tuberculosis.	Take considerable time to develop and validate, not timely for pandemic response. Causes weak disease symptoms	**4**							**4**
Other Types		Chimeras/Unknown	20							**20**
TOTAL			**176**	**9**	**6**	**1**	**0**	**0**		**192**

References

1. E. Dong, H. Du, L. Gardner, An interactive web-based dashboard to track COVID-19 in real time. *The Lancet infectious diseases*, (2020).
2. R. A. Khailany, M. Safdar, M. Ozaslan, Genomic characterization of a novel SARS-CoV-2. *Gene Rep* **19**, 100682-100682 (2020).
3. I. Astuti, Severe Acute Respiratory Syndrome Coronavirus 2 (SARS-CoV-2): An overview of viral structure and host response. *Diabetes & Metabolic Syndrome: Clinical Research & Reviews*, (2020).
4. S. Kang *et al.*, Crystal structure of SARS-CoV-2 nucleocapsid protein RNA binding domain reveals potential unique drug targeting sites. *Acta Pharmaceutica Sinica B*, (2020).
5. L. Du *et al.*, Priming with rAAV encoding RBD of SARS-CoV S protein and boosting with RBD-specific peptides for T cell epitopes elevated humoral and cellular immune responses against SARS-CoV infection. *Vaccine* **26**, 1644-1651 (2008).
6. S.-F. Wang *et al.*, Antibody-dependent SARS coronavirus infection is mediated by antibodies against spike proteins. *Biochemical and biophysical research communications* **451**, 208-214 (2014).
7. S.-J. Liu *et al.*, Immunological characterizations of the nucleocapsid protein based SARS vaccine candidates. *Vaccine* **24**, 3100-3108 (2006).
8. M. Czub, H. Weingartl, S. Czub, R. He, J. Cao, Evaluation of modified vaccinia virus Ankara based recombinant SARS vaccine in ferrets. *Vaccine* **23**, 2273-2279 (2005).
9. S. F. Ahmed, A. A. Quadeer, M. R. McKay, Preliminary identification of potential vaccine targets for the COVID-19 coronavirus (SARS-CoV-2) based on SARS-CoV immunological studies. *Viruses* **12**, 254 (2020).
10. Y. Wan *et al.*, Molecular Mechanism for Antibody-Dependent Enhancement of Coronavirus Entry. *Journal of Virology* **94**, (2019).
11. C.-T. Tseng *et al.*, Immunization with SARS coronavirus vaccines leads to pulmonary immunopathology on challenge with the SARS virus. *PloS one* **7**, e35421-e35421 (2012).
12. L. Liu *et al.*, Anti-spike IgG causes severe acute lung injury by skewing macrophage responses during acute SARS-CoV infection. *JCI Insight* **4**, e123158 (2019).
13. S. B. Halstead, Dengvaxia sensitizes seronegatives to vaccine enhanced disease regardless of age. *Vaccine* **35**, 6355-6358 (2017).
14. P. L. Acosta, M. T. Caballero, F. P. Polack, Brief History and Characterization of Enhanced Respiratory Syncytial Virus Disease. *Clin Vaccine Immunol* **23**, 189-195 (2015).
15. D. Tudor *et al.*, TLR9 pathway is involved in adjuvant effects of plasmid DNA-based vaccines. *Vaccine* **23**, 1258-1264 (2005).

16. J. M. Luke *et al.*, Coexpressed RIG-I Agonist Enhances Humoral Immune Response to Influenza Virus DNA Vaccine. *Journal of Virology* **85**, 1370 (2011).

17. F. Le Boeuf *et al.*, Reovirus FAST Protein Enhances Vesicular Stomatitis Virus Oncolytic Virotherapy in Primary and Metastatic Tumor Models. (10)(2e) *Ther Oncolytics* [illegible], (10)(2e)).

18. C. W. Brown *et al.*, The p14 FAST protein of reptilian reovirus increases vesicular stomatitis virus neuropathogenesis. *J Virol* **83**, 552-561 (2009).

19. P. Leblanc *et al.*, VaxCelerate II: rapid development of a self-assembling vaccine for Lassa fever. *Hum Vaccin Immunother* **10**, 3022-3038 (2014).

20. C. J. Mann *et al.*, Molecular signature of the immune and tissue response to non-coding plasmid DNA in skeletal muscle after electrotransfer. *Gene Therapy* **19**, 1177-1186 (2012).

21. N. Bessis, F. J. GarciaCozar, M. C. Boissier, Immune responses to gene therapy vectors: influence on vector function and effector mechanisms. *Gene Therapy* **11**, S10-S17 (2004).

22. T. Sugiyama *et al.*, CpG RNA: identification of novel single-stranded RNA that stimulates human CD14+CD11c+ monocytes. *J Immunol* **174**, 2273-2279 (2005).

23. R. Duncan, Fusogenic Reoviruses and Their Fusion-Associated Small Transmembrane (FAST) Proteins. *Annual Review of Virology* **6**, 341-363 (2019).

24. J. Read *et al.*, Reovirus FAST Proteins Drive Pore Formation and Syncytiogenesis Using a Novel Helix-Loop-Helix Fusion-Inducing Lipid Packing Sensor. *PLoS Pathog* **11**, e1004962 (2015).

25. M. Ciechonska, R. Duncan, Reovirus FAST proteins: virus-encoded cellular fusogens. *Trends in microbiology* **22**, 715-724 (2014).

26. D. Top, J. A. Read, S. J. Dawe, R. T. Syvitski, R. Duncan, Cell-cell membrane fusion induced by p15 fusion-associated small transmembrane (FAST) protein requires a novel fusion peptide motif containing a myristoylated polyproline type II helix. *J Biol Chem* **287**, 3403-3414 (2012).

27. S. Dawe, J. A. Corcoran, E. K. Clancy, J. Salsman, R. Duncan, Unusual topological arrangement of structural motifs in the baboon reovirus fusion-associated small transmembrane protein. *J Virol* **79**, 6216-6226 (2005).

28. S. Dawe, R. Duncan, The S4 genome segment of baboon reovirus is bicistronic and encodes a novel fusion-associated small transmembrane protein. *J Virol* **76**, 2131-2140 (2002).

29. J. A. Corcoran *et al.*, The p14 fusion-associated small transmembrane (FAST) protein effects membrane fusion from a subset of membrane microdomains. *J Biol Chem* **281**, 31778-31789 (2006).

30. H. Lv, S. Zhang, B. Wang, S. Cui, J. Yan, Toxicity of cationic lipids and cationic polymers in gene delivery. *Journal of Controlled Release* **114**, 100-109 (2006).

31. Z. Liu *et al.*, Composition and divergence of coronavirus spike proteins and host ACE2 receptors predict potential intermediate hosts of SARS-CoV-2. *Journal of medical virology* **92**, 595-601 (2020).

32. J. Nie *et al.*, Establishment and validation of a pseudovirus neutralization assay for SARS-CoV-2. *Emerging microbes & infections* **9**, 680-686 (2020).

33. H.-L. Xiong *et al.*, Robust neutralization assay based on SARS-CoV-2 S-bearing vesicular stomatitis virus (VSV) pseudovirus and ACE2-overexpressed BHK21 cells. *bioRxiv*, 2020.2004.2008.026948 (2020).

34. T. Thanh Le *et al.*, The COVID-19 vaccine development landscape. *Nature Reviews Drug Discovery* **19**, 305-306 (2020).

35. . (The Milken Institute, 2020).

36. F. Amanat, F. Krammer, SARS-CoV-2 Vaccines: Status Report. *Immunity* **52**, 583-589 (2020).

37. A. A. A. Aljabali, A. Berardi, D. J. Evans, in *Fundamentals of Nanoparticles,* A. Barhoum, A. S. Hamdy Makhlouf, Eds. (Elsevier, 2018), pp. 29-50.

38. J. F. C. Steele *et al.*, Synthetic plant virology for nanobiotechnology and nanomedicine. *Wiley Interdiscip Rev Nanomed Nanobiotechnol* **9**, (2017).

39. J. A. Kulkarni *et al.*, Design of lipid nanoparticles for in vitro and in vivo delivery of plasmid DNA. *Nanomedicine: Nanotechnology, Biology and Medicine* **13**, 1377-1387 (2017).

40. C. F. Cho *et al.*, Viral nanoparticles decorated with novel EGFL7 ligands enable intravital imaging of tumor neovasculature. *Nanoscale* **9**, 12096-12109 (2017).

41. J. Mriouah *et al.*, Abstract 5143: Fusogenic targeted liposomes: novel nanotherapy for specific treatment of prostate cancer. *Cancer Research* **77**, 5143-5143 (2017).

42. R. J. Paproski *et al.*, Porphyrin Nanodroplets: Submicron Ultrasound and Photoacoustic Contrast Imaging Agents. *Small* **In Press**, (2015).

43. C. F. Cho *et al.*, Molecular targeted viral nanoparticles as tools for imaging cancer. *Methods Mol Biol* **1108**, 211-230 (2014).

44. C. Perez-Medina *et al.*, A modular labeling strategy for in vivo PET and near-infrared fluorescence imaging of nanoparticle tumor targeting. *J Nucl Med* **55**, 1706-1711 (2014).

45. P. H. Beatty, J. D. Lewis, Cowpea mosaic virus nanoparticles for cancer imaging and therapy. *Adv Drug Deliv Rev*, (2019).

46. F. M. Brunel *et al.*, Hydrazone ligation strategy to assemble multifunctional viral nanoparticles for cell imaging and tumor targeting. *Nano Lett* **10**, 1093-1097 (2010).

47. H. S. Leong *et al.*, Intravital imaging of embryonic and tumor neovasculature using viral nanoparticles. *Nature protocols* **5**, 1406-1417 (2010).

48. J. D. Lewis *et al.*, Viral nanoparticles as tools for intravital vascular imaging. *Nat Med* **12**, 354-360 (2006).

49. A. L. Martin *et al.*, Synthesis of bombesin-functionalized iron oxide nanoparticles and their specific uptake in prostate cancer cells. *Journal of nanoparticle research : an interdisciplinary forum for nanoscale science and technology* **12**, 1599-1608 (2009).

50. Jazayeri, Poh, Development of Universal Influenza Vaccines Targeting Conserved Viral Proteins. *Vaccines* **7**, 169 (2019).

51. M. T. Koday *et al.*, Multigenic DNA vaccine induces protective cross-reactive T cell responses against heterologous influenza virus in nonhuman primates. *PLOS ONE* **12**, e0189780 (2017).

52. D. Hobernik, M. Bros, DNA Vaccines—How Far From Clinical Use? *International Journal of Molecular Sciences* **19**, 3605 (2018).

53. J. van Haasteren, S. C. Hyde, D. R. Gill, Lessons learned from lung and liver in-vivo gene therapy: implications for the future. *Expert opinion on biological therapy* **18**, 959-972 (2018).

54. C. S. Lee *et al.*, Adenovirus-mediated gene delivery: Potential applications for gene and cell-based therapies in the new era of personalized medicine. *Genes & Diseases* **4**, 43-63 (2017).

55. P. R. Cullis, M. J. Hope, Lipid Nanoparticle Systems for Enabling Gene Therapies. *Molecular Therapy* **25**, 1467-1475 (2017).

56. H. B. Parmar, R. Duncan, A novel tribasic Golgi export signal directs cargo protein interaction with activated Rab11 and AP-1-dependent Golgi-plasma membrane trafficking. *Mol Biol Cell* **27**, 1320-1331 (2016).

57. H. B. Parmar, C. Barry, R. Duncan, Polybasic trafficking signal mediates golgi export, ER retention or ER export and retrieval based on membrane-proximity. *PLoS One* **9**, e94194 (2014).

58. M. Ciechonska, R. Duncan, Lysophosphatidylcholine reversibly arrests pore expansion during syncytium formation mediated by diverse viral fusogens. *J Virol* **88**, 6528-6531 (2014).

59. J. A. Corcoran, E. K. Clancy, R. Duncan, Homomultimerization of the reovirus p14 fusion-associated small transmembrane protein during transit through the ER-Golgi complex secretory pathway. *J Gen Virol* **92**, 162-166 (2011).

60. E. K. Clancy, R. Duncan, Helix-destabilizing, beta-branched, and polar residues in the baboon reovirus p15 transmembrane domain influence the modularity of FAST proteins. *J Virol* **85**, 4707-4719 (2011).

61. E. K. Clancy, C. Barry, M. Ciechonska, R. Duncan, Different activities of the reovirus FAST proteins and influenza hemagglutinin in cell-cell fusion assays and in response to membrane curvature agents. *Virology* **397**, 119-129 (2010).

62. C. Barry, R. Duncan, Multifaceted sequence-dependent and -independent roles for reovirus FAST protein cytoplasmic tails in fusion pore formation and syncytiogenesis. *J Virol* **83**, 12185-12195 (2009).

63. D. Top, C. Barry, T. Racine, C. L. Ellis, R. Duncan, Enhanced fusion pore expansion mediated by the trans-acting Endodomain of the reovirus FAST proteins. *PLoS Pathog* **5**, e1000331 (2009).

64. E. K. Clancy, R. Duncan, Reovirus FAST protein transmembrane domains function in a modular, primary sequence-independent manner to mediate cell-cell membrane fusion. *J Virol* **83**, 2941-2950 (2009).

65. D. Top *et al.*, Liposome reconstitution of a minimal protein-mediated membrane fusion machine. *The EMBO journal* **24**, 2980-2988 (2005).

66. J. Salsman, D. Top, J. Boutilier, R. Duncan, Extensive syncytium formation mediated by the reovirus FAST proteins triggers apoptosis-induced membrane instability. *J Virol* **79**, 8090-8100 (2005).

67. R. Duncan, J. Corcoran, J. Shou, D. Stoltz, Reptilian reovirus: a new fusogenic orthoreovirus species. *Virology* **319**, 131-140 (2004).

68. J. A. C. Duncan, Reptilian Reovirus Utilizes a Small Type III Protein with an External Myristylated Amino Terminus To Mediate Cell-Cell Fusion. (2004).

69. J. A. Corcoran *et al.*, Myristoylation, a protruding loop, and structural plasticity are essential features of a nonenveloped virus fusion peptide motif. *J Biol Chem* **279**, 51386-51394 (2004).

70. J. A. Corcoran, R. Duncan, Reptilian reovirus utilizes a small type III protein with an external myristylated amino terminus to mediate cell-cell fusion. *J Virol* **78**, 4342-4351 (2004).

71. . (The World Health Organization), vol. 2020.

72. M. J. Mulligan *et al.*, Phase 1/2 Study to Describe the Safety and Immunogenicity of a COVID-19 RNA Vaccine Candidate (BNT162b1) in Adults 18 to 55 Years of Age: Interim Report. *medRxiv*, 2020.2006.2030.20142570 (2020).

73. K. S. Corbett *et al.*, SARS-CoV-2 mRNA Vaccine Development Enabled by Prototype Pathogen Preparedness. *bioRxiv*, 2020.2006.2011.145920 (2020).

74. F.-C. Zhu *et al.*, Safety, tolerability, and immunogenicity of a recombinant adenovirus type-5 vectored COVID-19 vaccine: a dose-escalation, open-label, non-randomised, first-in-human trial. *The Lancet* **395**, 1845-1854 (2020).

75. T. R. F. Smith *et al.*, Immunogenicity of a DNA vaccine candidate for COVID-19. *Nature Communications* **11**, 2601 (2020).

76. Q. Gao *et al.*, Development of an inactivated vaccine candidate for SARS-CoV-2. *Science*, (2020).

77. H. Wang *et al.*, Development of an inactivated vaccine candidate, BBIBP-CorV, with potent protection against SARS-CoV-2. *Cell*, (2020).

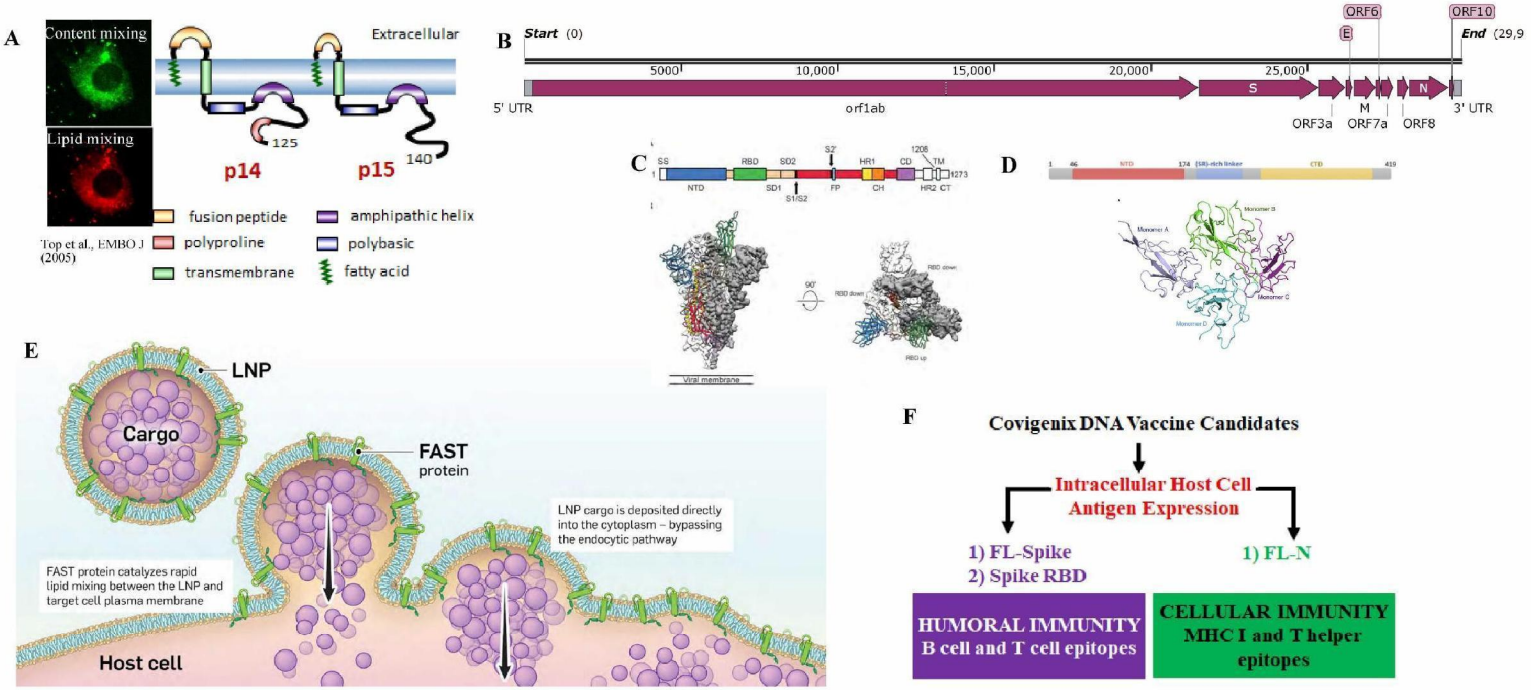
A
Content mixing
Lipid mixing
Extracellular
125
p14
p15
140
fusion peptide
polyproline
transmembrane
amphipathic helix
polybasic
fatty acid
Top et al., EMBO J (2005)
B
Start (0)
5000
10,000
15,000
20,000
25,000
S
E
M
N
ORF6
ORF10
End (29,9
5' UTR
orf1ab
ORF3a
ORF7a
ORF8
3' UTR
C
SS
RBD
SD2
S2'
HR1
CD
TM
1208
1273
NTD
SD1
S1/S2
FP
CH
HR2
CT
Viral membrane
RBD down
RBD up
90°
D
NTD
CTD
Monomer A
Monomer B
Monomer C
Monomer D
E
LNP
Cargo
FAST protein
LNP cargo is deposited directly into the cytoplasm – bypassing the endocytic pathway
FAST protein catalyzes rapid lipid mixing between the LNP and target cell plasma membrane
Host cell
F
Covigenix DNA Vaccine Candidates
Intracellular Host Cell Antigen Expression
1) FL-Spike
2) Spike RBD
1) FL-N
HUMORAL IMMUNITY
B cell and T cell epitopes
CELLULAR IMMUNITY
MHC I and T helper epitopes

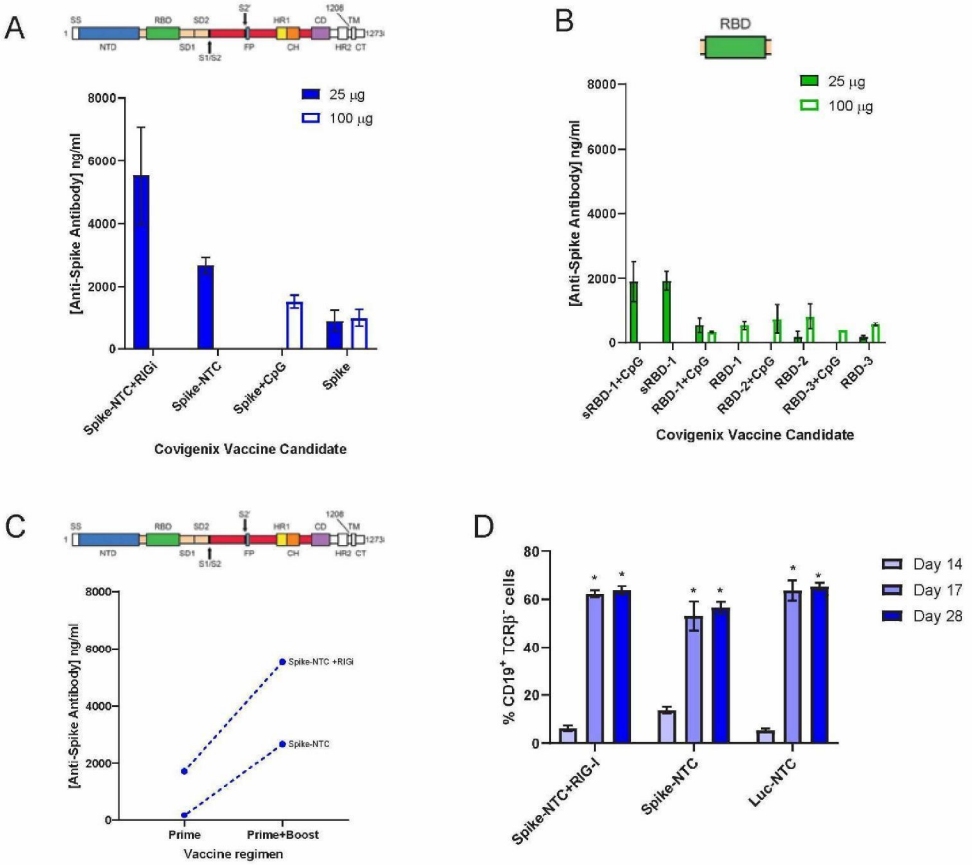

Fig 2. Antibody production induced by Covigenix vaccine candidates.

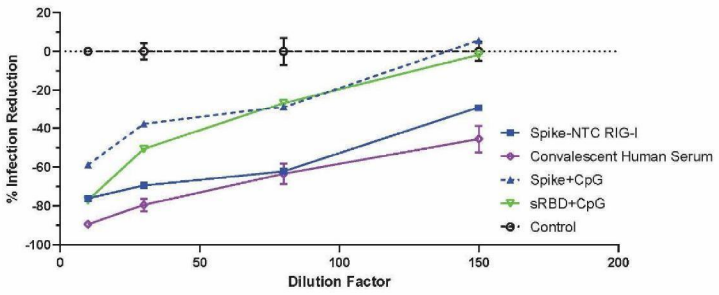

Fig.3. Psuedotyped VSV-GFP neutralization.

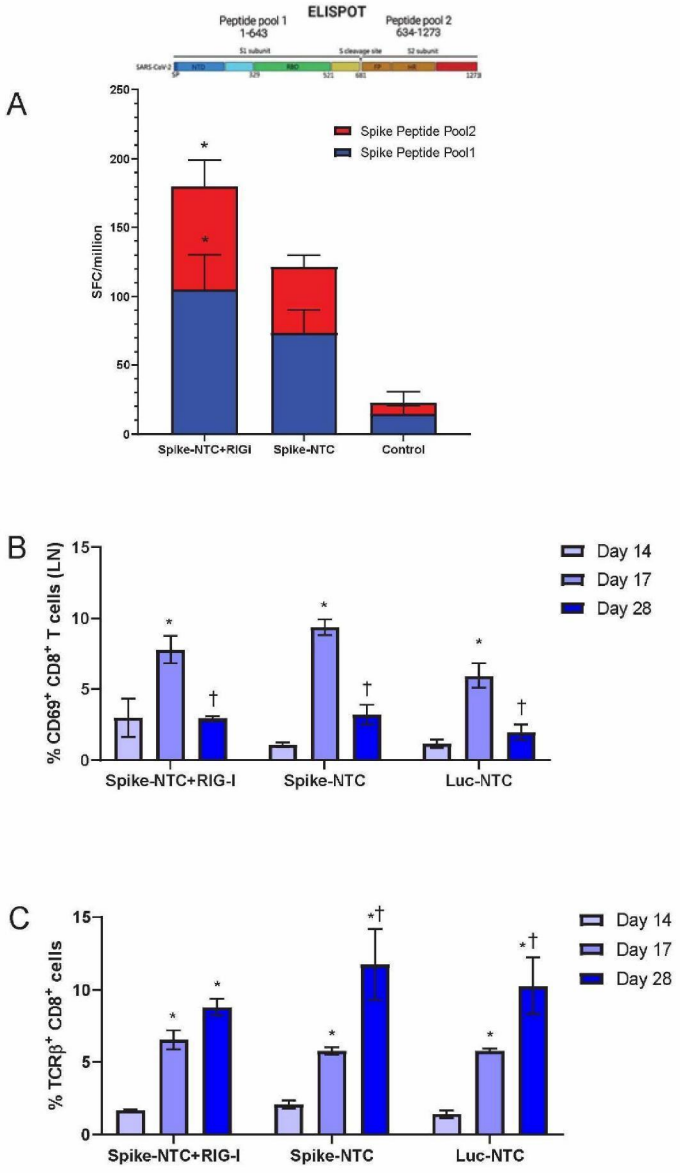

Fig 4. IFN- gamma ELISPOT.

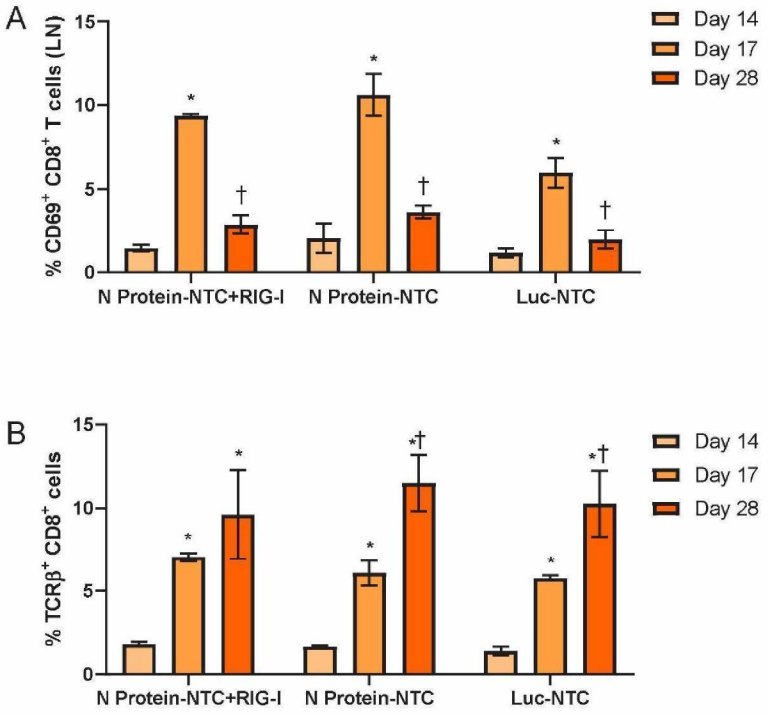
A
% CD69+ CD8+ T cells (LN)
15
10
5
0
Day 14
Day 17
Day 28
N Protein-NTC+RIG-I
N Protein-NTC
Luc-NTC
B
% TCRβ+ CD8+ cells
15
10
5
0
Day 14
Day 17
Day 28
N Protein-NTC+RIG-I
N Protein-NTC
Luc-NTC

Fig 5.